

Article

Nanocomposite PVDF Membrane for Battery Separator Prepared via Hot Pressing

Lukáš Plesník ^{1,*}, Karla Čech Barabaszová ¹, Sylva Holešová ¹, Pavlína Peikertová ¹, Gražyna Simha Martynková ¹ and Damian Stanislaw Nakonieczny ²

¹ Nanotechnology Centre, CEET, VŠB-Technical University of Ostrava, 17. listopadu 15/2172, 708 00 Ostrava, Czech Republic; karla.cech.barabaszova@vsb.cz (K.Č.B.); sylva.holesova@vsb.cz (S.H.); pavlina.peikertova@vsb.cz (P.P.); grazyna.simha@vsb.cz (G.S.M.)

² Department of Biomedical Engineering, Silesian University of Technology, Akademicka 2A, 44-100 Gliwice, Poland; damian.nakonieczny@polsl.pl

* Correspondence: lukas.plesnik@vsb.cz; Tel.: +420-0596-991-677

Abstract: Polyvinylidene fluoride (PVDF) is one of the materials most commonly used in membrane separators. The structures of pristine PVDF and PVDF nanocomposite films were processed via hot pressing at 140 °C, 170 °C, and 185 °C at a pressure of 2 tons for 15 min. According to a surface investigation using scanning electron microscopy (SEM), the spherulitic character of the PVDF nanocomposite films was preserved up to a pressing temperatures of 140 °C. The cross-sectional SEM images confirmed that higher pressing temperatures (170 °C) caused the structures to be compacted into monolithic films, and a pressing temperature of 185 °C caused the melting of the PVDF matrix and its recrystallization into thin films (21–29 µm). An average crystallinity value of 51.5% was calculated using differential scanning calorimetry (DSC), and this decreased as the pressing temperature increased. Fourier transform infrared (FTIR) measurements confirmed the presence of a dominant γ phases in the PVDF nanocomposite films, whose nanofillers consisted of vermiculite particles (ZnO_V and ZnO_V_CH) and mixed α + γ phases. The percentage of the electroactive γ phase (approximately 79%) was calculated via a FTIR analysis, and the ratio between the β phase and the α phase was determined from the Raman spectra. A hydrophilic surface with contact angles ranging from 61 to 84° was demonstrated for all the PVDF nanocomposite membranes. The superoleophilic surface was measured using poly(dimethylsiloxane) with contact angles ranging from 4 to 13°, and these angles reached lower values when in contact with sulfur particles.

Keywords: membrane separators; PVDF nanocomposite films; hot pressing; structural and phase characterization; hydrophilic and super oleophilic surfaces



Citation: Plesník, L.; Čech Barabaszová, K.; Holešová, S.; Peikertová, P.; Simha Martynková, G.; Nakonieczny, D.S. Nanocomposite PVDF Membrane for Battery Separator Prepared via Hot Pressing. *Batteries* **2023**, *9*, 398. <https://doi.org/10.3390/batteries9080398>

Academic Editor: Carlos Zieber

Received: 16 June 2023

Revised: 18 July 2023

Accepted: 29 July 2023

Published: 30 July 2023



Copyright: © 2023 by the authors. Licensee MDPI, Basel, Switzerland. This article is an open access article distributed under the terms and conditions of the Creative Commons Attribution (CC BY) license (<https://creativecommons.org/licenses/by/4.0/>).

1. Introduction

Membrane separators play an important role in many applications, from the food industry to the biomedical sector to energy applications. They can improve the purity of drinking water, serve as packaging material, contribute to tissue regeneration, and convert energy [1], and they are also used in the chemical, automotive, and electronic industries [1–3]. In each of these fields, the membranes have their own unique functions, which are often associated with their specific properties, such as thickness, porosity, thermal stability, wettability (hydrophobicity, oleophobicity, hemocompatibility), and mechanical and chemical properties (increased resistance to solvents and various cleaning agents, resistance to high temperatures or extreme pH conditions) [4].

With the increasing demand for energy storage devices, attention has been focused on the economic and ecological effects of individual components in recent lithium-ion batteries. Membrane separators are an important component of lithium-ion batteries as they separate the positive and negative electrodes, restrict the free passage of electrons, and prevent short-circuiting of the battery. The main function of a separator is the selective

separation of the metallic ions in the electrolyte, enabling them to migrate freely between the electrodes and restricting the large particles to maintain the shuttle effect [5]. The materials and structures of the membrane separators greatly affected the performance of lithium-ion batteries. There are three main types that are more common on the market today, namely microporous polymer membranes, nonwoven membranes, and inorganic composite membranes [6,7].

Polyvinylidene fluoride (PVDF) is one of the materials most frequently used in all of the membrane separator types listed above because of its remarkable thermal stability, high melting temperature, excellent chemical resistance, and high ionic conductivity [8]. The ionic conductivity of PVDF-based separators is higher than that of polyolefin materials because of the superior wettability of PVDF membrane separators [9]. The wettability of PVDF membrane separators refers to their ability to absorb the liquid electrolyte. A high wettability of the separator can improve the ionic conductivity of the battery and reduce the risk of short-circuits. On the other hand, low wettability that causes dendritic growth can cause poor performance and reliability issues during use, and it greatly affects both cell capacity and lifecycle. Optimizing the wettability of membrane separators is critical to ensure their efficiency in different applications [10,11].

Despite the potential of PVDF as a separator material, the design of PVDF separators still requires further optimization to ensure high performance and a long-lasting and reliable working life. Process parameters, such as temperature, pressure, and processing time, can significantly affect the properties of PVDF membrane separators, including their phase transformation, wettability, and so on [12]. One of the techniques that can determine the final properties of the membrane separator is hot press processing. Phase transformation is an important factor that affects the properties of membrane separators. PVDF is a semicrystalline polymer that can exist in different crystalline phases, including α , β , and γ phases. Since the β and γ phases are electroactive, due to their polarity, their presence is desirable in separators used in energy storage [13]. PVDF presents a very variable morphology that strongly depends on crystallization temperature and time [14]. Under conditions such as rising temperature, the pores of the separator are closed by the melting process, and the battery shuts down. For example, the polyethylene separator (PE) shuts the battery down when the core temperature reaches 130 °C, and this process will stop the transport of ions between the electrodes. If the battery does not shut down as the temperature rises, the heat in the failing cell could rise and lead to thermal runaway, causing the battery to overheat or even catch fire [4].

Additives can effectively induce polar phases in PVDF membranes, affecting the pore size distribution and the wettability of the membrane separators [11,15]. Many additives are used as porous barriers that allows some components to permeate and reject others (selective wettability). These membrane wettability filters are mostly superhydrophilic but oleophobic, or vice versa [16]. Inorganic additives, such as clay minerals and metal oxide nanoparticles, are relatively inexpensive and commercially available, and these have been widely investigated as nanofillers which can affect polymorphism, pore size distribution, spherulite size, and the wettability and mechanical properties of PVDF nanocomposite materials [17,18].

In previous work, we demonstrated that zinc oxide nanoparticles, zinc oxide nanoparticles_vermiculite, and zinc oxide nanoparticles_vermiculite_chlorhexidine can be used as nanofillers and incorporated into PVDF nanocomposite films, and we characterized the correlations between the microstructure, surface topography, and tribomechanical properties, and predicted their suitability for use as thin films in different applications [19]. Their structural variability and friction resistance (especially in the case of the zinc oxide nanoparticles_vermiculite_chlorhexidine nanofiller) in comparison with those of the pristine PVDF material led us to expand these nanocomposite materials for use as membrane separators. Their original structures were hot pressed at various temperatures to simulate the temperature and pressure field that is developed inside a lithium-ion battery. The suitability of these products for the separator parts of lithium-ion batteries was determined

based on the measurements of the wetting angles using a polydimethylsiloxane solution. Polydimethylsiloxane achieves high thermal stability at high and low temperatures, undergoes small temperature dependent viscosity changes, and is resistant to water. These properties make it suitable for use as a cooling medium in battery applications. In the case of battery damage due to exposure to heat or mechanical damage, the high wettability of the coolant relative to the separator can cause cooling and delayed chain reactions in batteries composed of multiple battery cells. When sulfur is added to the cooling medium (in this case, polydimethylsiloxane solution), the safety of the lithium-ion battery is higher. Sulfur can immobilize Li⁺ by reacting to form lithium polysulfides and thereby immobilizing metal cations. This can limit the chain reactions in battery cells in the event that the battery is damaged by burning or exposure to heat or mechanical damage [20].

In this paper, we discuss the effects of hot press processing on the structural and phase changes, thermal stability, and crystallinity of the PVDF nanocomposite separators, and we also monitor their wettability. Wettability is crucial for the design and optimization of membrane separators, and it is characterized here by three different solutions that simulate the relationship between hydrophilic and oleophobic properties. For this reason, the contact angle of pure poly(dimethylsiloxane) and poly(dimethylsiloxane) with a sulfur dispersion of 5 wt% was used to test the suitability of the pristine PVDF and PVDF nanocomposite film samples. The main goal of this work is to determine a binding temperature during hot pressing which will not lead to the thermal degradation of the polymer membranes, and to find out whether and how it affects the properties of the used nanofillers (zinc oxide nanoparticles, zinc oxide nanoparticles_vermiculite, and zinc oxide nanoparticles_vermiculite_chlorhexidine).

2. Materials and Methods

2.1. Preparation and Hot Pressing of PVDF and PVDF Nanocomposite Films

The pristine PVDF sample and the PVDF nanocomposite films were prepared using the solvent casting method. First, 1 g of PVDF granules (Sigma Aldrich) was dissolved in 10 mL of *N,N*-dimethylformamide (Sigma Aldrich, $M_w = 73,095$ g/mol) and 7 mL of acetone (Sigma Aldrich $M_w = 58,081$ g/mol) in a stirrer at 80 °C for 20 min before being transferred to an 11 cm diameter Petri dish and dried in an oven (Memmert) at a constant temperature of 140 °C for 24 h. The PVDF nanocomposite films were prepared under the same conditions, and the PVDF solution was enriched with 3 wt% of nanofiller and homogenized in an ultrasonic bath for 30 min. Zinc oxide nanoparticles (ZnO), zinc oxide nanoparticles_vermiculite (ZnO_V), and zinc oxide nanoparticles_vermiculite_chlorhexidine (ZnO_V_CH) were used as nanofillers. The prepared PVDF nanocomposite films were denoted as PVDF_ZnO, PVDF_ZnO_V, and PVDF_ZnO_V_CH, respectively. Details concerning the preparation and properties of the nanofillers and the PVDF nanocomposite films can be found in [19,21].

The hot pressing of the pure PVDF and the PVDF nanocomposite films was performed using a 25T Hydraulic Laminating Hot Press (MTI Corporation). Following this, 2 × 2 cm reference samples were cut from each film and pressed at a pressure of 2 tons for 15 min at 140, 170, and 185 °C. The hot-pressed films were then labelled in the following manner: PVDF_nanofiller type hot pressed temperature.

2.2. Characterization Methods

A scanning transmission electron microscope (STEM, JEOL JSM-7610F Plus, Tokyo, Japan) was used to investigate the morphologies of the surfaces and cross-sections of the pristine PVDF and PVDF nanocomposite films. The possibility of the appearance of nanofillers on the surface of the PVDF matrix was also investigated. The samples were coated with gold/palladium to avoid problems with electrical charging during microscopic observation. The SEM images were obtained using a secondary electron detector (SE, LEI). To characterize the cross-sections, the PVDF samples were immersed in liquid nitrogen for 15 s, broken in half, and coated with gold/palladium.

Differential scanning calorimetry (DSC) tests were performed using a DSC131 evo (Setaram, France) at temperatures from 0 to 200 °C and a heating rate of 5 °C/min under an argon atmosphere.

The FTIR spectra of the pristine PVDF and PVDF nanocomposite films were measured using the ATR (attenuated total reflectance, USA) technique. The samples were positioned and pressed with a fixing device on a single-reflection diamond ATR crystal. The FTIR spectra were collected using a Nicolet iS50 FTIR spectrometer (ThermoScientific, Waltham, MA, USA) with a DTGS detector on a Smart Orbit ATR accessory. The measurement conditions were as follows: spectral region: 4000–400 cm⁻¹; spectral resolution: 4 cm⁻¹; scans: 64; and Happ–Genzel apodization.

The Raman spectra were obtained using the Smart Raman system XploRA™ (Horiba, France). The intensity of the red laser (785 nm) was reduced to 10 mW and the acquisition time was set to 60 s and repeated 5 times. The spectra were collected at 10 different points 40 µm apart. The final spectra were normalized and an average spectrum was created in Origin Pro 9.1.

Three wettability tests were carried out: (1) distilled water contact angle (WCA) measurements; (2) pure poly(dimethylsiloxane) contact angle (PCA) measurements (LUKO-SIOL M, Lužební závody Kolín, Czech Republic); and (3) poly(dimethylsiloxane) (Sigma Aldrich) enriched with 5 wt% sulfur (Sigma Aldrich, powder, 99.98% trace metals basis, d_{m1} = 0.584 µm and d_{m2} = 15.17 µm) dispersion contact angle (PSCA) measurements. Poly(dimethylsiloxane) with 5 wt% of sulfur was prepared via vigorous magnetic stirring of 10 mL of poly(dimethylsiloxane) and water at a speed of 800 r/min for 30 min. The contact angles (CAs) of the pristine PVDF and PVDF nanocomposite films were measured using a three-point technique at 22.5 °C, 995 mba, and a relative humidity of 55%. A volume of 0.1 mL of solution drop was put onto the surface of the pristine PVDF and PVDF nanocomposite films using a micropipette. Each drop form was recorded using a Mitutoyo video camera (Tokyo, Japan), and the images were evaluated using the Pixel Fox program (Germany). The CAs examined are the results of 3 repeated measurements.

3. Results and Discussion

3.1. The Changes in the PVDF Nanocomposite Films after Hot Pressing

The pristine PVDF and PVDF nanocomposite films prepared using the solvent casting method with different nanofiller particles were investigated using a scanning electron microscope (SEM), images from which are shown in Figures 1 and 2. The fact that the film samples were prepared on the glass substrate of a Petri dish gave the opportunity to study both side surfaces. The morphology characteristics of “the top surface” of the film samples were observed; the opposite surface (the bottom surface) was that which was in contact with the glass substrate. In the case of cross-sectional characterization, for section profile measurements, the top surface is always shown in the upper right corner of the SEM image. For each samples, the film thickness and spherulitic diameter were evaluated from the SEM images using the JMicronVision image analyzer. The maximum and minimum values are shown in Table 1.

The pristine PVDF film was formed by regularly repeating hexagonal spherulitic grains with lamellar structures of uniform size in the range of 24.4–48.1 µm (width and length). From the cross-section images (Figure 1, second row), it is evident that the surface of the film is smooth where the film comes into contact with the glass substrate after casting. The shapes of the spherulitic grains are narrow in these places, and they widen towards the surface. It is probable that as a result of this, pores/cavities with an average size of 8 µm are formed between the grains, and these project on the surface as holes in the corners of the hexagons. The spherulitic grains themselves form regularly repeating lamellae without internal pores or defects.

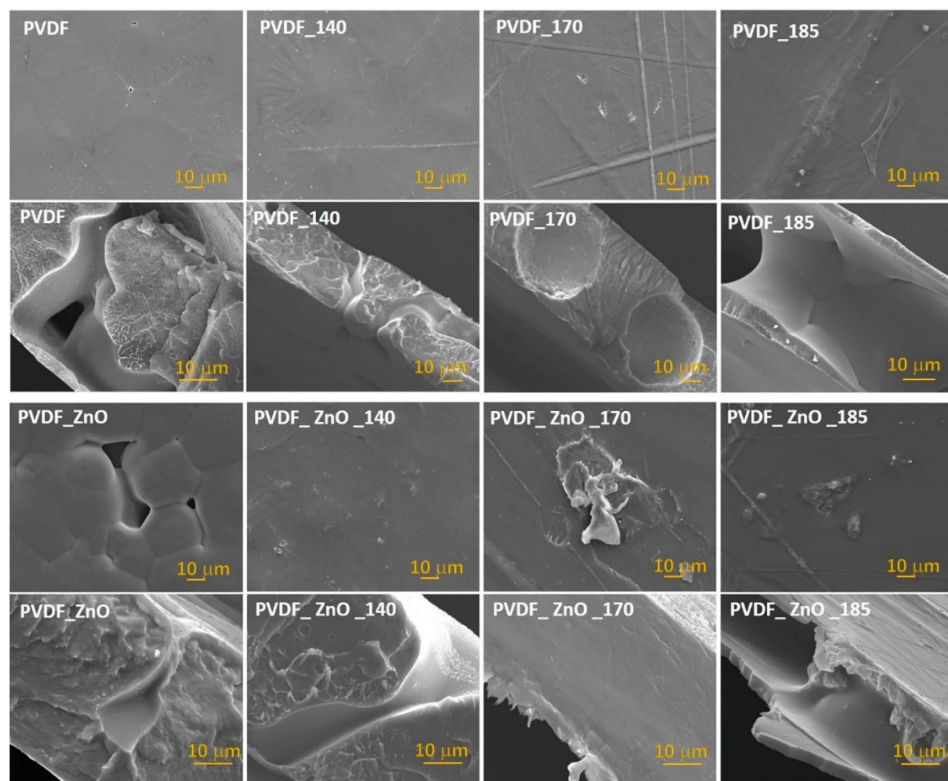


Figure 1. SEM images of the pristine PVDF and PVDF_xZnO surface morphologies (first rows) and cross-sections (second rows) before and after hot pressing (relevant heating temperatures are noted).

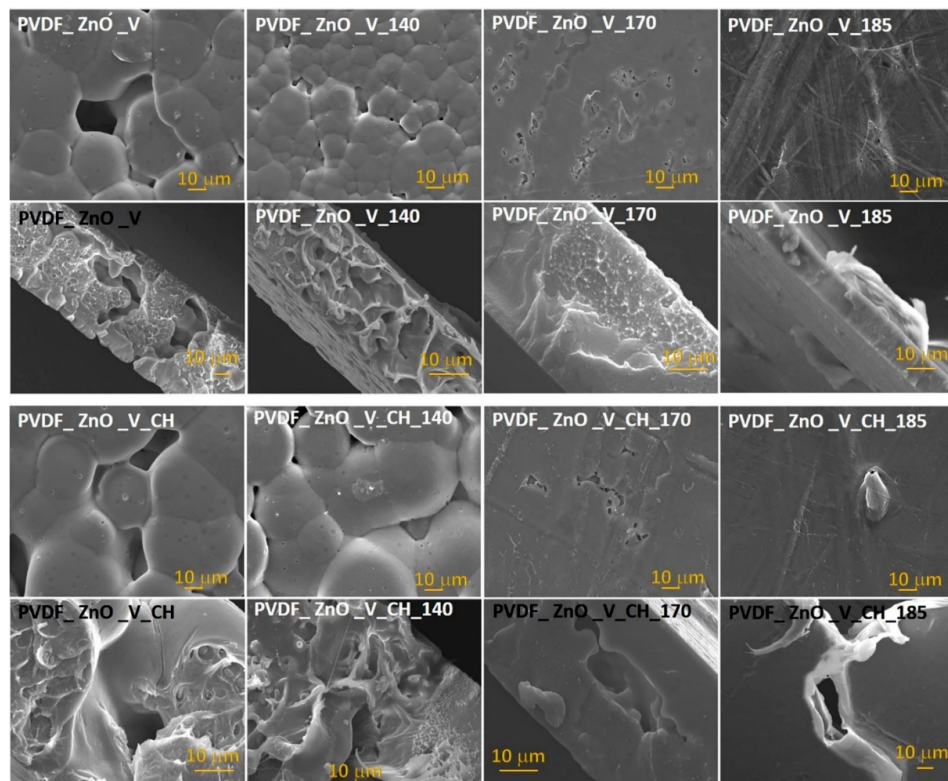


Figure 2. SEM images of the PVDF_xZnO_V and PVDF_xZnO_V_CH surface morphologies (first rows) and cross-sections (second rows) before and after hot pressing (relevant heating temperatures are noted).

Table 1. Minimum and maximum film thickness (t_{\min} , t_{\max}) and spherulitic diameter (d_{\min} , d_{\max}) of the pristine PVDF and PVDF nanocomposite films according to SEM measurements.

Sample	t_{\min}	t_{\max}	d_{\min} (μm)	d_{\max}
PVDF	42.3	47.5	24.4	48.1
PVDF_140	41.9	46.3	21.2	43.8
PVDF_170	63.1	65.1	4.1	7.6
PVDF_185	96.7	357.7	-	-
PVDF_ZnO	48.4	51.2	15.7	76.2
PVDF_ZnO_140	50.2	56.3	18.1	48.3
PVDF_ZnO_170	22.3	52.6	-	-
PVDF_ZnO_185	21.4	21.9	-	-
PVDF_ZnO_V	52.6	56.4	6.4	15.6
PVDF_ZnO_V_140	50.9	52.8	2.8	11.1
PVDF_ZnO_V_170	34.2	35.7	-	-
PVDF_ZnO_V_185	9.6	10.3	-	-
PVDF_ZnO_V_CH	57.6	62.7	18.0	44.6
PVDF_ZnO_V_CH_140	50.7	60.2	40.6	57.2
PVDF_ZnO_V_CH_170	38.0	39.3	-	-
PVDF_ZnO_V_CH_185	6.6	11.6	-	-

Hot pressing at 140 °C (PVDF_140 sample) preserved the size and hexagonal shape of the spherulitic grains. The individual grains were in close contact, without visible pores on the surface or inside the sample. The grains maintained an ordered crystalline character: the alternation of larger grains with smaller ones were repeated regularly.

The spherulitic structure of the PVDF matrix was suppressed via hot pressing at 170 °C (PVDF_170 sample). Spherulitic grains 4.1–7.6 μm in size occur sporadically (in places where film deformations occur) and are bounded by pores up to 2 μm in size. The surface of the PVDF_170 film is formed by deep grooves which were created by pressing the film through the scratched plate of the press. It can be seen from the cross-section images (see Figure 1) that the PVDF forms domains with an average size of 54.8 μm , and that these are dispersed throughout the entire volume of the PVDF matrix. The PVDF matrix itself is compact and forms lamellar cavities throughout its profile.

Hot pressing at 185 °C (PVDF_180 sample) caused the PVDF matrix to melt. The surface of the film was smooth and formed by deep grooves with deformed edges. An internal sandwich structure was observed. At the point of contact between the PVDF matrix and the press plates, the PVDF crystallized into thin films, the thickness of which did not exceed 2 μm on either side, and these formed large spherulitic grains exceeding 100 μm in size. Between these films, the PVDF crystallized to form smooth-walled crystal grains with voids larger than 50 μm between them.

Similar structural changes were observed in the PVDF_ZnO nanocomposite film (Figure 1, third row). The original spherulitic grains had irregular shapes (i.e., pentagons with sizes ranging from 15.7 to 76.2 μm). At the points of the contact between the large grains, cavities appeared irregularly along the entire length of their edges. From the cross-sectional images, it can be seen that the cavities reached half the thickness of the film. After thermal pressing (PVDF_ZnO_140 sample), the voids disappeared, appeared sporadically, or created holes in the entire film profile. The spherulitic grains were annihilated, and small grains recrystallized at the expense of large grains, reaching sizes of 18.1–48.3 μm . At the point of recrystallisation, the polymer formed recrystallisation residues on the surface that were similar to dust particles and did not exceed 3 μm in size.

From the profile image of the PVDF_ZnO_170 nanocomposite film, it can be seen that the sample formed a compact film with sharp edges. After pressing, there were defects and recrystallisation residues on the surface which reached sizes of up to 20 μm . The PVDF_ZnO_185 nanocomposite film was very thin and formed a sandwich structure with

cavities larger than 80 μm . The film was structurally heterogeneous, had cracks on the surface, and was very brittle.

The ZnO_V and ZnO_V_CH nanofillers caused a change in the size of the spherulitic grains in the original PVDF matrices (6.4–15.6 μm for the PVDF_ZnO_V film and 18.0–44.6 μm for the PVDF_ZnO_V_CH film) (Figure 2). This trend was also described in [22], where it was determined that clay platelets serve as effective nucleating sites for the polymer crystallites and cause a decrease in the size of spherulites. The spherulites formed irregular shapes, between which there were pores identical in size to the grains. While the surfaces of the spherulitic grains in all of the polymer nanocomposite films were smooth, the PVDF_ZnO_V_CH nanocomposite film had cavities of nonuniform size at the grain tops, and the edges of the grains were adjacent to each other. It can be seen from the profile images that while the PVDF_ZnO_V grains are compact and crystalline, the PVDF_ZnO_V_CH grains also form cavities/holes within their bulk.

Hot pressing at 140 $^{\circ}\text{C}$ contributed to the refinement of the spherulitic structure of the PVDF_ZnO_V_140 sample (to a grain size in the range of 2.8–11.1 μm), and, in contrast, to the unification and simultaneous increase in the size of the spherulitic grains to 40.6–57.2 μm . These grains had the most uniform shape, with rounded corners. When the nanocomposite films were broken after they were pulled out of liquid nitrogen, the subgrain boundaries were disrupted, leading to the formation of thin layers and nanofibers at their boundaries which indicated the non-negligible toughness of the polymer nanocomposites after embrittlement. The PVDF_ZnO_V_CH_140 nanocomposite film had spherical cavities and voids.

Hot pressing at 170 $^{\circ}\text{C}$ led to the complete suppression of the spherulitic structure and the formation of compact polymer plates with smooth surfaces formed by cavities (PVDF_ZnO_V_170) and voids (PVDF_ZnO_V_CH_170) of non-uniform size. Hot pressing at 185 $^{\circ}\text{C}$ completely deformed the profiles of the nanocomposite films as a result of the melting of the polymer matrices. The nanofiller particles visibly protruded from the polymer matrix onto its surface (PVDF_ZnO_V_185 and PVDF_ZnO_V_CH_185).

Table 1 shows the changes in the thickness (t) of the individual films expressed by the minimum and maximum measured values before and after thermal pressing. For each film, head pressing led to the unification of the thicknesses across the entire profile of the sample, resulting in a minimization of the dispersion of values between t_{\min} and t_{\max} . The thinnest films were prepared via hot pressing at 185 $^{\circ}\text{C}$, at which temperature the PVDF matrix melted, increasing the original area of the film, and recrystallized, thereby reducing its thickness. Due to the complete structural deformation, the thinnest thickness was measured for the PVDF_ZnO_V_CH_185 nanocomposite sample. In contrast, the strongest and highest thickness dispersion was observed for the PVDF_185 sample, and this was caused by the occurrence of holes and spherulitic grains inside the film.

3.2. DSC of the PVDF Nanocomposite Films

Differential scanning calorimetry (DSC) was used to determine the maximum melting temperatures and crystallinities of the PVDF films. The degree of crystallinity (X_c) was calculated using the following Equation (1)

$$X_c(\%) = \frac{\Delta H_m}{w_{\text{PVDF}} \times \Delta H_m^0} \cdot 100 \quad (1)$$

where ΔH_m is the specific melting enthalpy of the sample, w_{PVDF} is the weight percentage of the PVDF, and ΔH_m^0 is the melting enthalpy of the 100% crystalline polymer matrix (104.6 J/g for PVDF) [23]. The results of the DSC analysis are shown in Table 2.

Table 2. Thermal analysis of pristine PVDF and PVDF nanocomposite films.

Sample	T _{max} (°C)	ΔH _m (J/g)	X _c (%)
PVDF	169.3	43.0	42.4
PVDF_140	167.6	51.5	50.8
PVDF_170	170.3	54.9	54.1
PVDF_185	168.1	55.6	54.8
PVDF_ZnO	171.6	52.4	51.7
PVDF_ZnO_140	168.3	56.2	55.4
PVDF_ZnO_170	170.2	49.5	48.8
PVDF_ZnO_185	168.1	47.8	47.1
PVDF_ZnO_V	171.5	52.4	51.7
PVDF_ZnO_V_140	171.1	56.0	55.1
PVDF_ZnO_V_170	180.0	51.9	51.1
PVDF_ZnO_V_185	168.4	48.9	48.2
PVDF_ZnO_V_CH	171.2	71.2	70.2
PVDF_ZnO_V_CH_140	170.9	51.8	51.1
PVDF_ZnO_V_CH_170	178.5	45.6	45.0
PVDF_ZnO_V_CH_185	168.0	47.1	46.5

For the pristine PVDF samples, it was observed that hot pressing did not significantly change the melting temperature (T_{max}), which ranged between 167.6 and 170.3 °C. However, there was an increase in their crystallinity (X_c), which increased as the pressing temperature increased. The pristine PVDF had a crystallinity value of 42.4%, and after hot pressing this value increased to 54.8%. For the samples containing ZnO particles, there was also no significant change in the melting temperature due to hot pressing. The PVDF_ZnO sample reached a crystallinity of 51.7%. After pressing at 140 °C (PVDF_ZnO_140), the highest crystallinity of 55.4% was achieved. When it was pressed at a higher temperature, the crystallinity value decreased. The samples containing the ZnO_V and ZnO_V_CH nanofillers pressed at 170 °C had a maximum melting temperature of about 180 °C. The crystallinity of the ZnO_V-modified samples did not change significantly from that of the original sample after temperature pressing (these ranged from 48.2 to 55.1%). The unheated PVDF_ZnO_V_CH sample had the highest crystallinity (70.2%). After hot pressing, the crystallinity significantly decreased.

The results of DSC analysis show that each nanofiller increases the crystallinity of the PVDF in the sample. In particular, the nanofillers containing ZnO_V_CH significantly increased the crystallinity from 42.4 to 70.2%. After the hot pressing of the samples containing ZnO and ZnO_V, the crystallinity increased at 140 °C, but when the process was performed at a higher temperature, the crystallinity decreased. The opposite was the case with the pure PVDF, the crystallinity of which increased at higher process temperatures. The sample that yielded the filler combined with the organic compound CH lost significant crystallinity after the hot-pressing process.

The high crystallinity (higher than 40%) exhibited by nanocomposite films is one of the major reasons for the relatively high internal resistance of some lithium-ion batteries. Because the crystalline region of the polymer film hinders the migration of lithium ions, batteries with these membranes often exhibit low charge/discharge capacity [6]. It can be assumed that due to their higher crystallinity percentage (more than 50%), the prepared PVDF nanocomposite materials are suitable for use in membrane separators. Higher crystallinity was achieved here via the type of nanofiller that was applied, the preparation method (the solvent casting method), and the hot-pressing process. At the same time, the hot-pressing process noticeably decreased the crystallinity of all the nanofillers.

3.3. FTIR of the PVDF Nanocomposite Films

The Fourier transform infrared (FTIR) technique is a very useful tool which can provide information about the structures of semicrystalline PVDF polymers which exist in three basic distinct polymorphs and allow us to distinguish between them. The results of the FTIR analysis were mainly used to monitor the phase characterization of the semicrystalline PVDF polymer, which is most commonly found in α , β , and γ phases. The FTIR spectra are shown in Figures 3 and 4, and the evaluated phases, the fractions of electroactive phases (F_{EA}), and the most intense FTIR peaks are reported in Table 3.

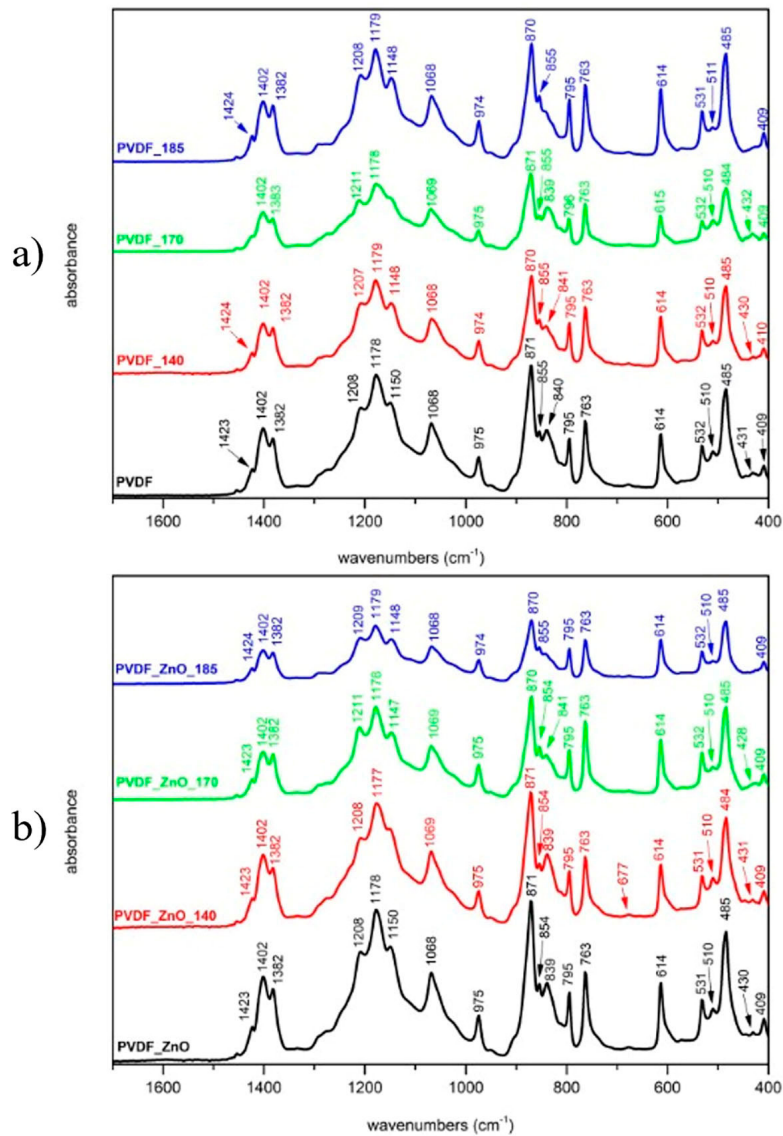


Figure 3. FTIR spectra of the (a) pristine PVDF and (b) PVDF_xZnO nanocomposite films before and after hot pressing.

The phase types of the studied samples were determined via FTIR analysis, in which each phase is represented by peaks of known wavenumbers. The α phase is predominantly determined by bands at 614 and 763 cm^{-1} corresponding to CF_2 bending and skeletal bending vibrations. The β phase is represented by a vibration at 1275 cm^{-1} which is attributed to C-F out-of-plane deformation [24]. The γ phase is mainly characterized by a band at 1234 cm^{-1} , which is attributed to CF out-of-plane deformation, and by peaks at 483 and 833 cm^{-1} . All of the samples contained both α and γ phases before heat treatment, except the PVDF_xZnO_V sample, where the presence of the nanofiller caused

the formation of the γ phase only. The PVDF and PVDF_ZnO samples were still made up of α and γ phases after hot pressing at all temperatures. The PVDF_ZnO_V sample consisted exclusively of the γ phase, which was supplemented by the α phase after pressing at 185 °C. The PVDF_ZnO_V_CH sample was created via a mixture of α and γ phases. After hot pressing at 140 and 170 °C, this sample occurred exclusively in the γ phase, but after hot pressing at 185 °C, the γ phase was converted to the α phase [24,25].

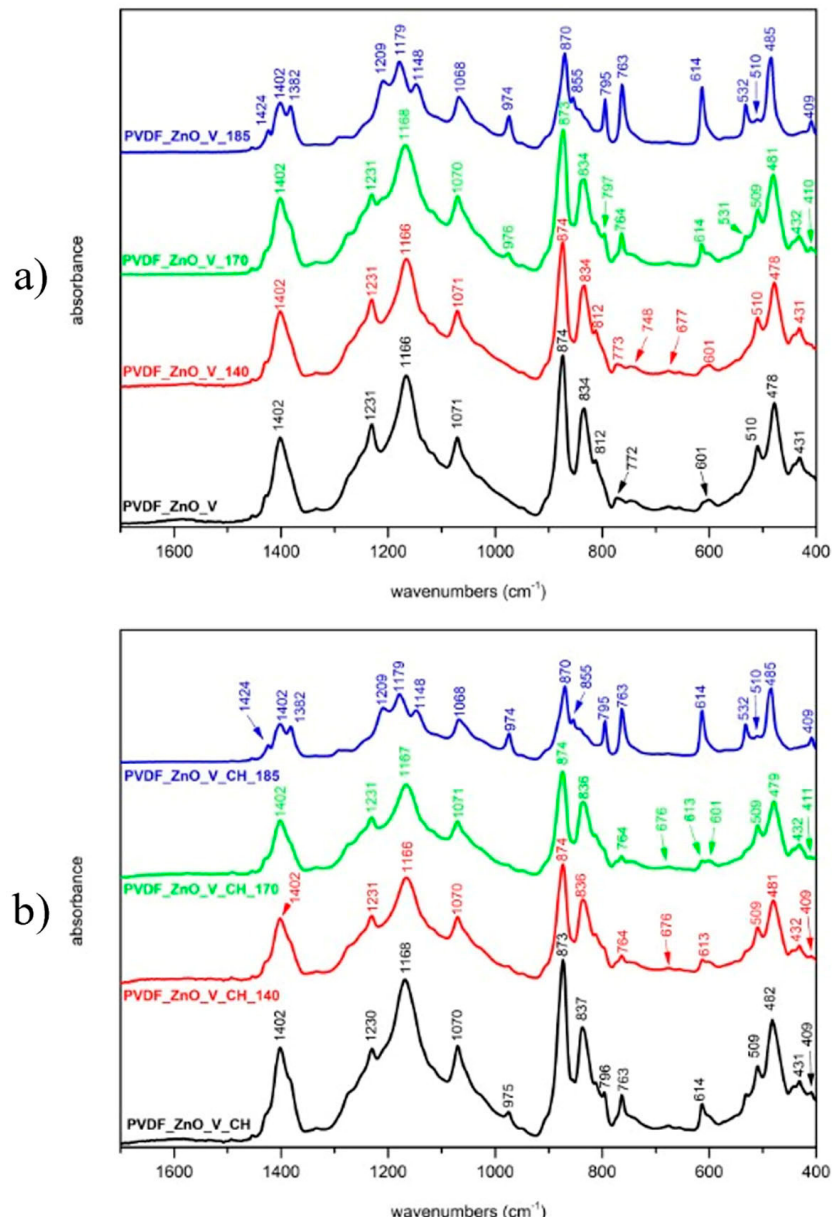


Figure 4. FTIR spectra of the (a) PVDF_ZnO_V and (b) PVDF_ZnO_V_CH nanocomposite films before and after hot pressing.

These polymeric materials are being studied because of their potential for use as separators in batteries, and their electroactivity is suitable for this type of application. The β and γ phases have electroactive properties, so their contributions were determined by the characteristic peak at 840 cm⁻¹ in the samples. The fractions of the electroactive phases (F_{EA}) in the samples were calculated using Equation (2):

$$F_{EA} = \frac{A_{EA}}{\left(\frac{K_{EA}}{K_\alpha}\right)A_\alpha + A_{EA}} \cdot 100 \quad (2)$$

where A_{EA} and A_α are the absorbance of each phase and $K_{EA} (7.7 \cdot 10^4 \text{ cm}^2 \cdot \text{mol}^{-1})$ and $K_\alpha (6.1 \cdot 10^4 \text{ cm}^2 \cdot \text{mol}^{-1})$ are the absorbance coefficients [13].

Table 3. PVDF phases present in the pristine PVDF and PVDF nanocomposite films according to FTIR and Raman measurements.

Sample	Phases	F _{EA} (%)	Peaks (cm ⁻¹)	$\frac{\beta}{\alpha} (-)$
PVDF	$\alpha + \gamma$	41.52	614, 763, 431, 485	0.31
PVDF_140	$\alpha + \gamma$	35.91	614, 763, 430, 485	0.27
PVDF_170	$\alpha + \gamma$	42.55	615, 763, 432, 484	0.31
PVDF_185	$\alpha + \gamma$	35.19	614, 763, 485	0.21
PVDF_ZnO	$\alpha + \gamma$	41.43	614, 763, 430, 485	0.23
PVDF_ZnO_140	$\alpha + \gamma$	45.45	614, 763, 431, 484	0.24
PVDF_ZnO_170	$\alpha + \gamma$	31.44	614, 763, 428, 485	0.32
PVDF_ZnO_185	$\alpha + \gamma$	35.91	614, 763, 485	0.21
PVDF_ZnO_V	γ	79.37	431, 478, 812, 834, 1231	N/A
PVDF_ZnO_V_140	γ	78.74	431, 478, 812, 834, 1231	N/A
PVDF_ZnO_V_170	γ	63.77	432, 481, 834, 1231	1.12
PVDF_ZnO_V_185	$\alpha + \gamma$	34.15	614, 763, 485, 1231	0.19
PVDF_ZnO_V_CH	$\alpha + \gamma$	65.79	614, 763, 431, 482, 1230	N/A
PVDF_ZnO_V_CH_140	γ	69.53	432, 481, 1231	N/A
PVDF_ZnO_V_CH_170	γ	71.94	432, 479, 1231	N/A
PVDF_ZnO_V_CH_185	α	34.60	614, 763	N/A

3.4. Raman Spectroscopy of the PVDF Nanocomposite Films

The measured Raman spectra in all the samples correspond to PVDF. The bands' shift is within 5 cm⁻¹, which is not significant. In the samples from the PVDF group, no shift was observed, and in the two other groups (the PVDF_ZnO and PVDF_ZnO_V samples), little shifts were observed, and these may be connected to the presence of ZnO and vermiculite. To distinguish the three possible PVDF polymorphs (α , β , and γ), only the 650–950 cm⁻¹ region is shown in Figure 5 [26].

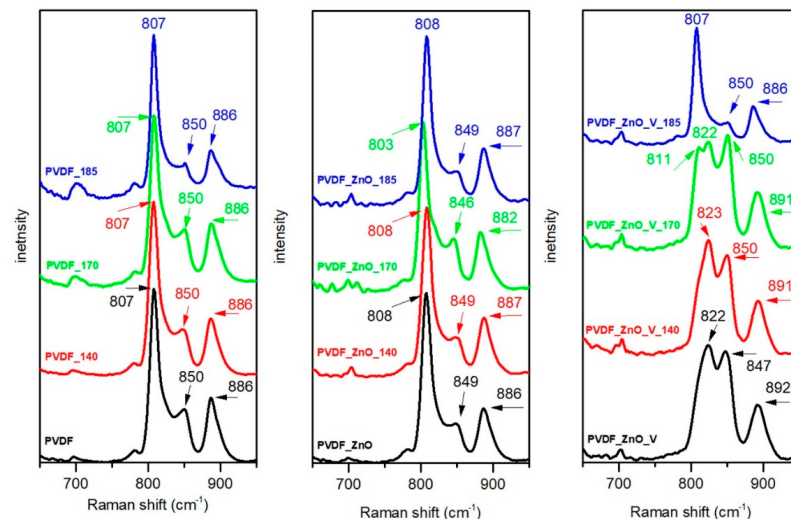


Figure 5. Normalized average Raman spectra of the pristine PVDF, PVDF_ZnO, and PVDF_ZnO_V nanocomposite films before and after hot pressing.

In the PVDF samples, the α phase prevailed (the bands at 807 and 886 cm⁻¹ correspond to the α phase) [26–28]. β phase was also visible in Raman spectra (850 cm⁻¹) [27,28]. In contrast, the γ phase (822 cm⁻¹) was not visible in the average Raman spectra, but it was present in some of the measured points as a shoulder (two points in the PVDF sample, one point in the PVDF_140 sample, and one point in the PVDF_170 sample) or regular band (one point in the PVDF_185 sample). In the PVDF_185 sample, no γ phase was observed.

This was the same for other groups of samples (PVDF_ZnO and PVDF_ZnO_V), where the γ phase was not observed in the sample that underwent the highest temperature treatment. Among the PVDF_ZnO samples, the γ phase was only visible in the PVDF_ZnO_170 at two points (in the regular band and in the shoulder). In contrast, in the PVDF_ZnO_V, PVDF_ZnO_V_140, and PVDF_ZnO_V_170 samples, the γ phase dominated, and this is in accordance with the FTIR measurements. Unfortunately, very high fluorescence occurred in the PVDF_ZnO_V_CH group during the Raman measurements, and therefore no spectra with visible Raman bands were obtained.

Furthermore, a quantitative analysis of the β phase relative to the α phase can be carried out using Equation (3) [26,29]:

$$\frac{\beta}{\alpha} = \frac{I(\beta)}{I(\alpha)} = \frac{I_{850\text{cm}^{-1}}}{I_{807\text{cm}^{-1}}} \quad (3)$$

The calculated values of the ratios between the β phase and the α phase are presented in Table 3. When the ratio is higher than 1, the α phase is in the minority. When the PVDF_ZnO_V and PVDF_ZnO_V_140 samples are excluded (no bands for the α phase at $\sim 807\text{ cm}^{-1}$ were visible), the β phase predominates in relation to the α phase in only one case (PVDF_ZnO_V_170). The sample with the lowest amount of β phase was the PVDF_ZnO_V_185 sample, whose the ratio was only 0.19.

3.5. Contact Angles of the PVDF Nanocomposite Films

The contact angle (CA) was measured for three solutions: 1) distilled water (WCA); 2) pure poly(dimethylsiloxane) (PCA); and 3) poly(dimethylsiloxane) with 5 wt% sulfur (PSCA) dispersion. The poly(dimethylsiloxane) with 5 wt% sulfur was prepared via vigorous magnetic stirring of 10 mL poly(dimethylsiloxane) at a speed of 800 r/min for 30 min. The contact angles (CAs) of the pristine PVDF and PVDF nanocomposite films are summarized in Figure 6.

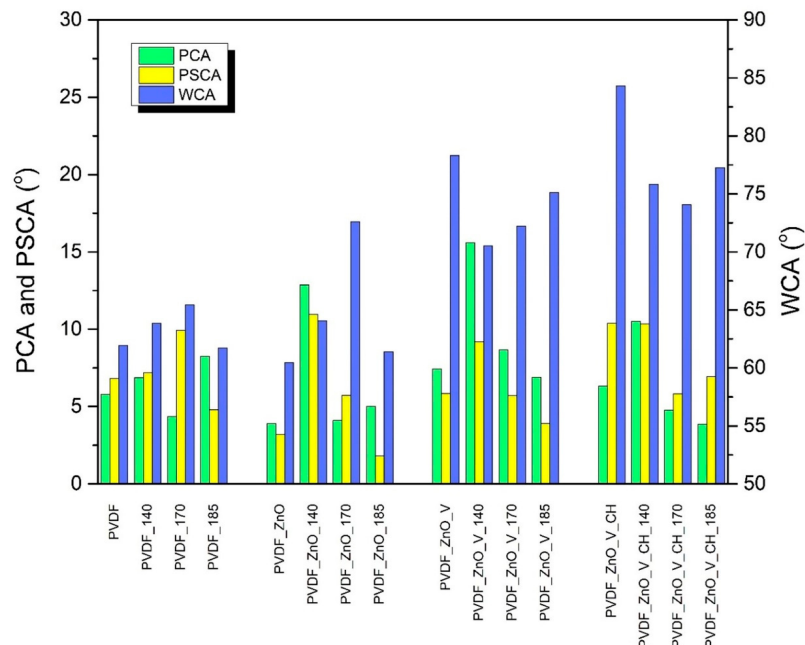


Figure 6. Contact angles of the distilled water (WCA), poly(dimethylsiloxane) liquid (PCA), and poly(dimethylsiloxane) with 5 wt% sulfur (PSCA) dispersion for the pristine PVDF and PVDF nanocomposite films before and after hot pressing.

The WCA values confirmed that the surfaces of all PVDF films were wettable (hydrophilic), and the WCA value measured for the original PVDF film was 61.9° . The

nanofillers in the PVDF caused increases in the WCA values (up to 78.3° for the PVDF_ZnO_V samples and up to 84.3° for the PVDF_ZnO_V_CH samples). In contrast, for the PVDF_ZnO samples, the WCA value was lower (60.5°), probably as a consequence of the different sizes of the spherulitic grains and the higher compatibility of the spherulitic grains of the film. The consistent upward character of the WCA values (which did not exceed 65°) was achieved via hot pressing. Only for the PVDF_ZnO_170 sample was there a WCA value of 72.6° , and this can be attributed to the compact nature of the sample. Higher WCA values were measured for the PVDF_ZnO_V and PVDF_ZnO_V_CH samples, and this confirmed their very fine spherulitic structure and higher degree of crystallinity. The hot-pressing process caused a drop in the WCA values from 70.5° to 77.3° , and the PVDF_ZnO_V_140 and PVDF_ZnO_V_170 samples reached lower values. This can be attributed to the more uniform size of the spherulitic grains and the reduction in the number of pores between them.

The PCA and PSCA values were significantly lower than the WCA values, ranging from 3.2° to 12.9° . The exception was the PVDF_ZnO_V_140 sample, for which the PCA value reached 15.6° . A slight increase in the CA was also observed in the PVDF nanocomposite films formed by nanofillers with vermiculite. Vermiculite particles are characterized by a high adsorption capacity which allows them to absorb the liquid component into their interspace. They also perform a barrier function when, in connection with the higher density of the pure poly(dimethylsiloxane) dispersion, they prevent the penetration of the tested solution into the PVDF structure. Slightly higher PSCA values were measured compared with the PCA values. Due to the fact that the sulfur particles in the poly(dimethylsiloxane) solution are made up of two size fractions ($d_{m1} = 0.584 \mu\text{m}$ and $d_{m2} = 15.17 \mu\text{m}$, d_m is mode size), we can assume that during contact between the solution and the surface of the PVDF film, the fine fraction penetrates into the pores and spaces while the larger fraction subsequently adheres to the surface and contributes to an increase in the PSCA values.

4. Conclusions

The novel polyvinylidene fluoride (PVDF) nanocomposite films with 3 wt% of zinc oxide nanoparticles (ZnO), zinc oxide_vermiculite (ZnO_V), and/or zinc oxide_vermiculite_chlorhexidine (ZnO_V_CH) as nanofillers were press at 140°C , 170°C , and 185°C at a pressure of 2 tons for 15 min. The main reason of the hot press was to simulate the conditions of mechanical and thermal loading in lithium-ion batteries and to help predict structural and phase changes in the PVDF matrix with regard to the changes in the wettability properties of the PVDF nanocomposite films.

The spherulitic structures of the pristine PVDF and PVDF nanocomposite membranes were preserved in all the PVDF samples up to a pressing temperature of 140°C . The largest spherulitic grains with a significant number of pores between them were characterized in the pristine PVDF and PVDF_ZnO ($30\text{--}50 \mu\text{m}$) samples; in the PVDF_ZnO_V and PVDF_ZnO_V_CH samples, the spherulitic grains were smaller ($15\text{--}45 \mu\text{m}$). The hot press at 140°C led to uniformity in grain size and a minimal number of pores. The thicknesses of these films ranged from 42 to $56 \mu\text{m}$. Hot pressing at temperatures of 170°C and 185°C caused the suppression of the appearance of spherulitic grains, and, in the PVDF samples, the character of monolithic films (170°C). Pressing at 185°C caused the PVDF matrix to melt and recrystallize into thin films ($21\text{--}9 \mu\text{m}$).

The structural changes coincided with changes in the average crystallinity values, which reached 42–55% for the pristine PVDF and PVDF_ZnO samples, while for the PVDF_ZnO_V and PVDF_ZnO_V_CH samples they were in the 45–70% range. For all the PVDF nanocomposite films that were hot pressed at 140°C , the crystallinity values decreased as the pressing temperature increased (only for the pristine PVDF samples did the crystallinity increase).

The crystallization of both the α and γ phases of the PVDF nanocomposite films was evaluated. While for the pristine PVDF and PVDF nanocomposites with ZnO nanofillers, the mixed phases ($\alpha + \gamma$) prevailed, in the case of the ZnO_V nanofillers, it was only the

γ phase. Only in the PVDF_ZnO_V_CH_185 sample was the α phase approved. In this sample, there was a total structural change in the membrane film, i.e., the complete recrystallisation of the PVDF matrix into a very thin film (9 μm). It is evident that vermiculite particles played a critical role in the resulting crystalline phases in the PVDF nanocomposite films. The characteristic peak for the β phase (in the case of the PVDF matrices) at 840 cm^{-1} was used to determine the percentages of the electroactive phases, which were calculated using the FTIR analyses (these were highest—approximately 79%—in the PVDF_ZnO_V and PVDF_ZnO_V_140 samples).

Wettability was characterized using the contact angle measurements of the three types of liquid. All the PVDF nanocomposite membranes had hydrophilic surfaces. The presence of vermiculite particles and the sizes of the spherulitic grains were shown to have a positive effect and lead to higher hydrophilicity (PVDF_ZnO_V_CH: WCA = 84°). The lowest hydrophilicity was measured for the pristine PVDF and PVDF_ZnO, for which the WCA was 61°. The pressing temperature had no effect on the WCA values; only in the samples with vermiculite were there decreases in WCA values (decreases of approximately 10%). The poly(dimethylsiloxane) and poly(dimethylsiloxane) with 5 wt% sulfur produced superoleophilic surfaces with contact angles ranging from 4 to 13° in all the PVDF samples, regardless of hot pressing.

In general, it can be concluded that the PVDF nanocomposite films presented in this paper are suitable membrane materials. It was found that hot pressing at 140 °C positively affected the properties (e.g., thermal stability and wettability) of the PVDF nanocomposite films.

Author Contributions: Conceptualization, K.Č.B.; investigation, K.Č.B., L.P. and P.P.; formal analysis, L.P. and S.H.; writing—original draft preparation, L.P. and K.Č.B.; writing—review and editing, K.Č.B., S.H., G.S.M. and D.S.N. All authors have read and agreed to the published version of the manuscript.

Funding: This work was supported by the project No. SP2023/026 (“Smart nanomaterials for energy storage and savings”).

Data Availability Statement: Not applicable.

Acknowledgments: The authors thank G. Kratošová for the SEM micrographs and K. Hrabovská for the loan of the contact angle measuring device.

Conflicts of Interest: The authors declare no conflict of interest.

References

- Pal, P.; Chaurasia, S.P.; Upadhyaya, S.; Kumar, R.; Sridhar, S. Development of hydrogen selective microporous PVDF membrane. *Int. J. Hydrogen Energy* **2020**, *45*, 16965–16975. [[CrossRef](#)]
- Manikandan, S.; Subbaiya, R.; Saravanan, M.; Ponraj, M.; Selvam, M.; Pugazhendhi, A. A critical review of advanced nanotechnology and hybrid membrane based water recycling, reuse, and wastewater treatment processes. *Chemosphere* **2022**, *289*, 132867. [[CrossRef](#)] [[PubMed](#)]
- Sanaeepur, H.; Amooghin, A.E.; Shirazi, M.M.A.; Pishnamazi, M.; Shirazian, S. Water desalination and ion removal using mixed matrix electrospun nanofibrous membranes: A critical review. *Desalination* **2022**, *521*, 115350. [[CrossRef](#)]
- Luo, W.; Cheng, S.; Wu, M.; Zhang, X.; Yang, D.; Rui, X. A review of advanced separators for rechargeable batteries. *J. Power Sources* **2021**, *509*, 230372. [[CrossRef](#)]
- Jang, J.; Oh, J.; Jeong, H.; Kang, W.; Jo, C. A Review of Functional Separators for Lithium Metal Battery Applications. *Materials* **2020**, *13*, 4625. [[CrossRef](#)] [[PubMed](#)]
- Song, Y.; Sheng, L.; Wang, L.; Xu, H.; He, X. From separator to membrane: Separators can function more in lithium ion batteries. *Electrochim. Commun.* **2021**, *124*, 106948. [[CrossRef](#)]
- Cheng, B.; Li, Z.; Li, Q.; Ju, J.; Kang, W.; Naebe, M. Development of smart poly(vinylidene fluoride)-graft-poly(acrylic acid) tree-like nanofiber membrane for pH-responsive oil/water separation. *J. Membr. Sci.* **2017**, *534*, 1–8. [[CrossRef](#)]
- Yanilmaz, M.; Lu, Y.; Dirican, M.; Fu, K.; Zhang, X. Nanoparticle-on-nanofiber hybrid membrane separators for lithium-ion batteries via combining electrospraying and electrospraying and electrospinning techniques. *J. Membr. Sci.* **2014**, *456*, 57–65. [[CrossRef](#)]
- Zhang, W.; Tu, Z.; Qian, J.; Choudhury, S.; Archer, L.A.; Lu, Y. Design principles of functional polymer separators for high-energy, metal-based batteries. *Small* **2018**, *14*, 1703001. [[CrossRef](#)]

10. Wu, D.; Deng, L.; Sun, Y.; Teh, K.S.; Shi, C.; Tan, Q.; Zhao, J.; Sun, D.; Lin, L. A high-safety PVDF/Al₂O₃ composite separator for Li-ion batteries via tip-induced electrospinning and dip-coating. *RSC Adv.* **2017**, *7*, 24410–24416. [[CrossRef](#)]
11. Francis, C.F.; Kyriatzi, I.L.; Best, A.S. Lithium-Ion Battery Separators for Ionic-Liquid Electrolytes: A Review. *Adv. Mater.* **2020**, *32*, 1904205. [[CrossRef](#)]
12. Tarbuttona, J.; Leb, T.; Helfrichb, G.; Kirkpatrickb, M. Phase Transformation and Shock Sensor Response of Additively Manufactured Piezoelectric PVDF. *Procedia Manuf.* **2017**, *10*, 982–989. [[CrossRef](#)]
13. Vasic, N.; Steinmetz, J.; Görke, M.; Sinapius, M.; Hühne, C.; Garnweinert, G. Phase Transitions of Polarised PVDF Films in a Standard Curing Process for Composites. *Polymers* **2021**, *13*, 3900. [[CrossRef](#)]
14. Gregorio, R.; Capitao, R.C. Morphology and phase transition of high melt temperature crystallized poly(vinylidene fluoride). *J. Mater. Sci.* **2000**, *35*, 299–306. [[CrossRef](#)]
15. Wang, X.; Chen, D.; He, T.; Zhou, Y.; Tian, L.; Wang, Z.; Cui, Z. Preparation of Lateral Flow PVDF Membrane via Combined Vapor and Non-Solvent-Induced Phase Separation (V-NIPS). *Membranes* **2023**, *13*, 91. [[CrossRef](#)]
16. Wang, B.; Li, J.; Wang, G.; Liang, W.; Zhang, Y.; Shi, L.; Guo, Z.; Liu, W. Methodology for Robust Superhydrophobic Fabrics and Sponges from In Situ Growth of Transition Metal/Metal Oxide Nanocrystals with Thiol Modification and Their Applications in Oil/Water Separation. *ACS Appl. Mater. Interfaces* **2013**, *5*, 1827–1839. [[CrossRef](#)]
17. Liu, T.; Yuan, J.; Zhen, Y.; Zhang, C.; Li, Y. Porous poly(vinylidene fluoride) (PVDF) membrane with 2D vermiculite nanosheets modification for non-aqueous redox flow batteries. *J. Membr. Sci.* **2022**, *651*, 120468. [[CrossRef](#)]
18. Čech Barabaszová, K.; Holešová, S.; Hundáková, M.; Hrabovská, K.; Plesník, L.; Kimmer, D.; Joszko, K.; Gzik-Zroska, B.; Basiaga, M. Antimicrobial PVDF nanofiber composites with the ZnO-vermiculite-chlorhexidine based nanoparticles and their tensile properties. *Polym. Test.* **2021**, *103*, 107367. [[CrossRef](#)]
19. Čech Barabaszová, K.; Holešová, S.; Plesník, L.; Kolská, Z.; Joszko, K.; Gzik-Zroska, B. Hybrid Nanofillers Creating the Stable PVDF Nanocomposite Films and Their Effect on the Friction and Mechanical Properties. *Polymers* **2022**, *14*, 3831. [[CrossRef](#)]
20. Caixia, L.; Xi, Z.; Guo, D.; Chen, X.; Yin, L. Chemical Immobilization Effect on Lithium Polysulfides for Lithium-Sulfur Batteries. *Small* **2018**, *14*, 1701986. [[CrossRef](#)]
21. Čech Barabaszová, K.; Holešová, S.; Šulcová, K.; Hundáková, M.; Thomasová, B. Effects of Ultrasound on Zinc Oxide/Vermiculite/Chlorhexidine Nanocomposite Preparation and Their Antibacterial Activity. *Nanomaterials* **2019**, *9*, 1309. [[CrossRef](#)] [[PubMed](#)]
22. Patro, T.U.; Mhalgi, M.V.; Khakhar, D.V.; Misra, A. Studies on poly(vinylidene fluoride)-clay nanocomposites: Effect of different clay modifiers. *Polymer* **2008**, *49*, 3486–3499. [[CrossRef](#)]
23. Indolia, A.P.; Gaur, M.S. Investigation of structural and thermal characteristics of PVDF/ZnO nanocomposites. *J. Therm. Anal. Calorim.* **2013**, *113*, 821–830. [[CrossRef](#)]
24. Bormashenko, Y.; Pogreb, R.; Stanevsky, O.; Bormashenko, E. Vibrational spectrum of PVDF and its interpretation. *Polym. Test.* **2004**, *23*, 791–796. [[CrossRef](#)]
25. Xiaomei, C.; Tingping, L.; Daoheng, S.; Liwei, L. A critical analysis of the α , β and γ phases in poly(vinylidene fluoride) using FTIR. *RSC Adv.* **2017**, *7*, 15382–15389. [[CrossRef](#)]
26. Shepelin, A.; Glushenkov, A.M.; Lussini, V.C.; Fox, P.J.; Dicinoski, G.W.; Shapter, J.G.; Ellis, A.V. New Developments in Composites, Copolymer Technologies and Processing Techniques for Flexible Fluoropolymer Piezoelectric Generators for Efficient Energy Harvesting. *Energy Environ. Sci.* **2019**, *4*, 1143–1176. [[CrossRef](#)]
27. Chapron, D.; Rault, F.; Talbourdet, A.; Lemort, G.; Cochrane, C.; Bourson, P.; Devaux, E.; Campagne, C. In-situ Raman Monitoring of the Poly(vinylidene fluoride) crystalline structure during a melt-spinning process. *J. Raman Spectrosc.* **2021**, *52*, 1073–1079. [[CrossRef](#)]
28. Silva, M.P.; Sencadas, V.; Rolo, A.G.; Botelho, G.; Machado, A.V.; Rocha, J.G.; Lanceros-Méndez, S. Influence of the Crystallization Kinetics on the Microstructural Properties of γ -PVDF. *Mater. Sci. Forum* **2008**, *587–588*, 534–537. [[CrossRef](#)]
29. Riosbass, M.T.; Loh, K.J.; O'Bryan, G.; Loyola, B.R. In Situ Phase Change Characterization of PVDF Thin Films Using Raman Spectroscopy. *Proc. SPIE* **2014**, *9061*, 90610Z. [[CrossRef](#)]

Disclaimer/Publisher's Note: The statements, opinions and data contained in all publications are solely those of the individual author(s) and contributor(s) and not of MDPI and/or the editor(s). MDPI and/or the editor(s) disclaim responsibility for any injury to people or property resulting from any ideas, methods, instructions or products referred to in the content.